Reliability of Raman measurements of thermal conductivity of single-layer graphene due to selective electron-phonon coupling: A first-principles study

Ajit K. Vallabhaneni, Dhruv Singh, Hua Bao, Jayathi Murthy, and Xiulin Ruan

Phys. Rev. B **93**, 125432 — Published 28 March 2016

DOI: 10.1103/PhysRevB.93.125432

Is Raman Measurement of Thermal Conductivity of Single Layer Graphene and Other 2D Materials Reliable?

Ajit K Vallabhaneni[1,2] Dhruv Singh[3], Hua Bao[4], Jayathi Murthy[5,2], Xiulin Ruan[1,2,*]

[1] School of Mechanical Engineering Purdue University, West Lafayette, IN, USA
[2] BIRCK Nanotechnology Center Purdue University West Lafayette, IN, USA
[3] Process Technology modeling, Intel Corporation Hillsboro, OR, USA
[4] University of Michigan –Shanghai Jiao Tong University Joint Institute, Shanghai Jiao Tong University, Shanghai, China
[5] Department of Mechanical Engineering University of Texas at Austin, Austin, TX, USA

[*]Corresponding author: ruan@purdue.edu

ABSTRACT

Raman spectroscopy has been widely used to measure thermal conductivity (κ) of 2D materials such as graphene. This method is based on a well-accepted assumption that different phonon polarizations are in near thermal equilibrium. However, in this work we show that in laser irradiated single layer graphene, different phonon polarizations are in strong non-equilibrium, using predictive simulations based on first principles density functional perturbation theory (DFPT) and a multi-temperature model. We first calculate the electron cooling rate due to phonon scattering as a function of the electron and phonon temperatures, and the results clearly illustrate that optical phonons dominate the hot electron relaxation process. We then use these results in conjunction with the phonon scattering rates computed using perturbation theory to develop a multi-temperature model, and resolve the spatial temperature distributions of the energy carriers in graphene under steady state laser irradiation. Our results show that electrons, optical phonons, and acoustic phonons are in strong non-equilibrium, with the ZA phonons showing the largest non-equilibrium to other phonon modes, mainly due to their weak coupling to other carriers in suspended graphene. Since ZA phonons are the main heat carriers in graphene, we estimate that neglecting this non-equilibrium leads to under-estimation of thermal conductivity in experiments at room temperature by a factor of 1.35 to 2.6, depending on experimental conditions and assumptions used. Under-estimation is also expected in Raman measurements of other 2D materials when the optical-acoustic phonon coupling is weak.

1. Introduction

Raman spectroscopy [1] is widely used in experiments to measure various properties of graphene [2] and other 2D materials [3] like the number of layers [2, 4], defect concentration [4], optical phonon temperature [5], and thermal conductivity[6-9]. This process involves coupling between various energy carriers including photons, electrons, and phonons within the single layer graphene (SLG) as shown in Fig. 1. Figure 1 (a) shows a schematic of the Raman spectroscopy experiments done on suspended graphene. Subsequent to laser irradiation, the excited electrons rapidly (within few tens of fs) attain the equilibrium Fermi-Dirac distribution corresponding to a high temperature by e-e scattering [10]. These hot electrons relax by scattering with the in-plane phonons near the Γ and K points in the Brillouin zone (BZ), and the resulting hot phonons subsequently relax by scattering with other phonon groups with intermediate wave vector and out-of-plane polarization.

In the current work, we focus only on the thermal conductivity (κ) measurement of single layer graphene (SLG) using Raman spectroscopy. The thermal conductivity of SLG from these measurements varies from 660 W/mK – 5850 W/mK [5, 6, 11, 12]. In these experiments, temperature is measured either by the shift in the Raman peak frequency[11, 12] or by the ratio of intensities of stokes to anti-stokes[5]. While the temperature measured in the former case is associated with intermediate-frequency phonons including both acoustic and optical phonons[13], temperature in the latter case clearly corresponds to that of the high frequency optical phonon[5]. In both cases, the measured temperature is then assumed to be the equilibrium lattice temperature, and is used to derive κ from the Fourier model. Since all phonon modes contribute to thermal conductivity, such an approach is valid only when different phonon modes are in local thermal equilibrium, and would be invalid in the presence of strong non-equilibrium [14]. Recent experiments on graphene using Raman spectroscopy have revealed that electrons are in near-equilibrium with optical phonons under high power densities although the uncertainty in experimental measurements is over 100 K [15]. However, Chae *et al*. found that the optical phonons are not in equilibrium with the intermediate frequency phonons based on a similar experimental setup [16]. Since the derived κ is inversely proportional

to the temperature difference between the laser spot and the contacts (ambient temperature), it is important

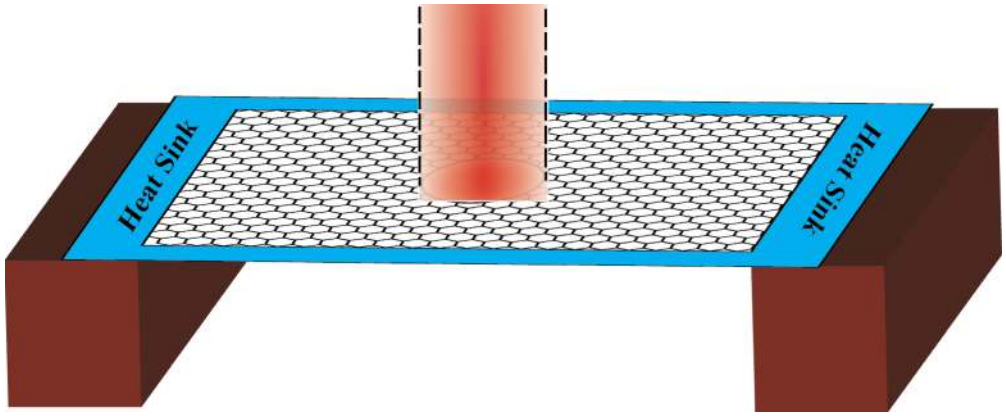

(a)

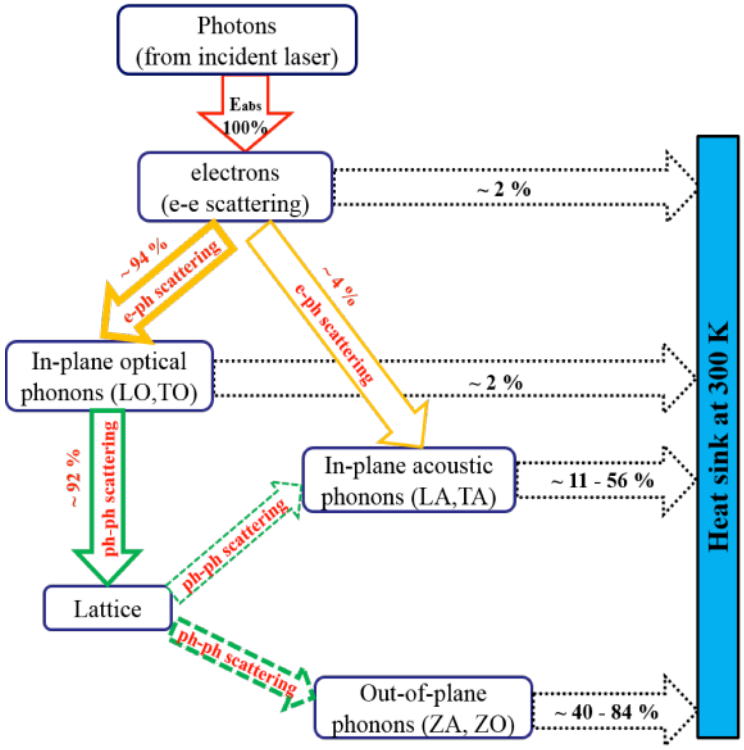

(b)

Figure 1. (a) Schematic of Raman spectroscopy experiment on suspended graphene. (b) Flow chart showing the typical flow of energy among the carriers in laser-irradiated graphene along with percentage of input energy that is being diffused out to the heat sink at 300 K. (The thickness of arrows in color is proportional to the magnitude of energy received from other carriers). These percentages are calculations in this work, and the details are presented below.

to assess the equilibrium assumption in light of the above mentioned studies. However, measuring the temperatures of all the individual phonon polarizations is almost impossible in experiments. On the other hand, theoretical modeling would require high-fidelity prediction of scattering and transport of electrons, optical phonons, and acoustic phonons. Although electron scattering rates and hot electron cooling rates

have been predicted using the first-principles approach, the results have not been used together with phonon-phonon scattering rates and carrier transport theories to assess the degree of energy carrier non-equilibrium in Raman spectroscopy.

The primary objective of this work is to resolve the spatial temperature distributions of all the energy carriers and assess their degree of non-equilibrium in laser-irradiated single layer graphene at steady state. A two-temperature molecular dynamics [17] approach can resolve non-equilibrium between electrons and phonons but not among different phonon modes. Therefore, in this work we have extended the two-temperature model to a multi-temperature mode as to be detailed later. This is achieved by calculating the e-ph scattering rates from first principles, and then solving their coupled transport in conjunction with ph-ph scattering rates (calculated earlier by us using perturbation theory). Our results, as shown in Fig. 1 (b), indicate that hot electrons relax mainly through optical phonon emission, which accounts for approximately 94 % of the energy loss. However, due to their low group velocity, they subsequently pass the energy to acoustic phonons. Near the heat sink, the majority of heat flow rate is carried by acoustic phonons, especially ZA phonons (40-85%). Essentially, the decoupling between the energy receiver (optical phonon) and the energy transporter (ZA phonons), as well as the weak coupling between ZA and other phonon modes leads to strong non-equilibrium among the phonon modes and renders the Raman measurement of thermal conductivity of SLG unreliable. These percentages were calculated in this work, and the details of calculations are presented below.

2. Simulation Methodology

Our work starts with the first-principles calculations of e-ph coupling strength in graphene. Park *et al* have calculated the electron scattering rates in intrinsic and doped graphene using the first-principles approach [18]. Various groups have also adopted similar methodologies to calculate the electron scattering rates, estimate the corresponding deformation potential (DP) parameters for e-ph interaction [19], and subsequently to use them to calculate the electron cooling rates as a function of T_e and T_{ph} [20]. In this work, we calculate all the important parameters mentioned above, including the electron scattering rate (τ^{-1}), mobility (μ), electrical conductivity (σ), electron thermal conductivity (κ) and the rate of energy exchange

between electrons and phonons ($E_{e\text{-}ph}$), directly from first principles without any empirical parameters or assumptions for the e-ph coupling strength. The last parameter is of prime importance in the current work as it determines the rate of energy transfer from electrons to each of the phonon groups.

A Monkhorst-Pack grid of 96×96×1 is chosen to discretize the entire first Brillouin zone (BZ) of graphene based on the two-atom unit cell with an equilibrium lattice constant of 2.435 Å [21]. A vacuum space of 10 Å is left in the out-of-plane direction to avoid any interaction between the periodic images. Only the valence electrons are treated explicitly using a plane-wave basis with an energy cutoff of 75 Ry, whereas the core electrons are modeled using Norm-conserving pseudo-potentials. The LDA approximation is used to model the exchange-correlation interactions. Phonons are treated as a perturbation to the equilibrium structure in DFPT and the corresponding derivatives of the self-consistent potential are calculated using linear response theory. The DFT/DFPT calculations in this study are performed using the Quantum-Espresso package [22]. In DFT, the e-ph coupling element for an event where an electron at initial state $|i,k\rangle$ is scattered to $|j,k+q\rangle$ by a phonon mode of wave vector q and polarization v, where i,j are the electronic branch indices and k is the wave vector, is defined using the expression shown below

$$g_{k,q}^{\nu} = \sqrt{\frac{\hbar}{2M\omega_q^{\nu}}} \left\langle j,k+q \left| \nabla V_q^{\nu} \right| i,k \right\rangle \tag{1}$$

Here, $\hbar$ is the reduced Planck's constant, M is the mass of carbon atom, ω_q^v is the corresponding frequency of the phonon, ΔV_q^v represents the first-order change in the SCF potential of the ground state due to the perturbation along the corresponding phonon eigen vector. After validating the magnitude of parameter 'g', we used it to calculate the scattering rate and cooling rates of electrons.

3. Results and Discussion

To verify our method, we first calculated the magnitude of square of the e-ph coupling element 'g' averaged over the two linear bands for electrons at the Dirac point ('K') due to the optical phonons at Γ and K ($|g|^2_{avg}$). Figure 2 shows this variation with phonon wave vector q for a K electron interacting

with each of the four in-plane phonon modes along Γ – K. The value of $|g|^2_{avg}$ is 0.0405 eV^2 for the doubly degenerate E_{2g} mode, and 0.0989 eV^2 for the TO mode at the K point. These are in excellent agreement with values reported in the literature previously (0.0405 eV^2 and 0.0994 eV^2) [23]. It can also be noted from the inset that g^2_{avg} of acoustic modes increases almost linearly near Γ and as the wave vector (q) increases, phonons lose their long wavelength nature (TA loses it sooner than LA), and as a result $|g|^2_{avg}$ drops [24]. The interaction of electrons with out-of-plane phonons (ZA, ZO) is negligible due to reflection symmetry.

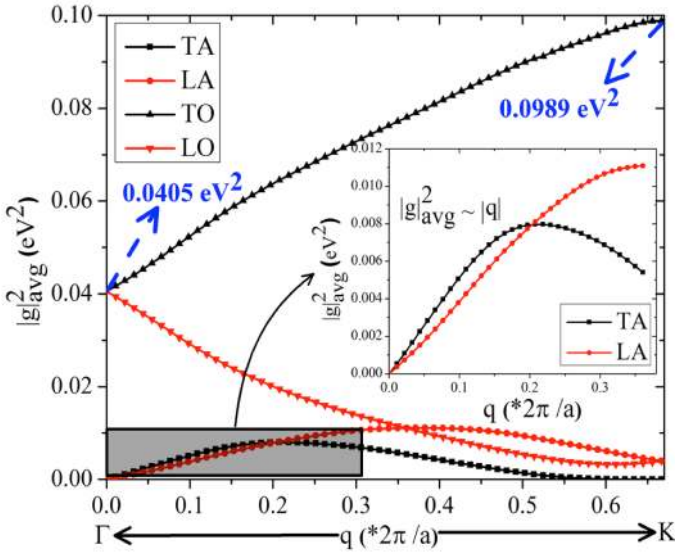

Figure 2. Variation of $|g|^2_{avg}$ for each of the in-plane phonon modes along the high-symmetry direction (Γ-K). The inset shows the variation for acoustic phonon modes near Γ.

After calculating the coupling matrix elements, we calculate the electron scattering rates due to four different phonon groups which are significant for e-ph scattering using the Fermi's golden rule (FGR). They are Γ-LO/TO, Γ- LA/TA, K-TO and K-LO/LA. The scattering rate of an electron state $|i,k\rangle$ where i is the branch index and k is the wave vector, is denoted by the $1/\tau_{ik}$ and is given by the following expression:

$$\frac{1}{\tau_{ik}}(T) = \sum_{j,\nu,q} |\, g^{\nu}_{k,q}\,|^2 \left[\begin{array}{l} \left\{ (f_{j,k+q} + N^{\nu}_q)\delta(\varepsilon_{j,k+q} - \varepsilon_{i,k} - \omega^{\nu}_q) \right\} \\ + \left\{ (1 + N^{\nu}_q - f_{j,k+q})\delta(\varepsilon_{j,k+q} - \varepsilon_{i,k} + \omega^{\nu}_q) \right\} \end{array} \right] \qquad (2)$$

where $g_{k,q}$ is the e-ph coupling matrix element defined above and i,j are the electron branch indices, T is the temperature at which the equilibrium electron and phonon distribution functions (f and N respectively) are evaluated (300 K in this case), ε is the corresponding electronic state energy, v is the polarization of the phonon at wave vector q, and ω_{qv} is its corresponding frequency, $f_{j,k+q}$ is the equilibrium Fermi-Dirac (F-D) distribution evaluated as $\{=1/[\exp(\varepsilon_{j,k+q}/K_bT)+1]\}$, N_q is the equilibrium Bose-Einstein (B-E) distribution evaluated as $\{=1/[\exp(\hbar\omega_{qv}/K_bT)-1]\}$, and K_b is the Boltzmann constant. The derivation of this expression is presented in the supplemental information. The matrix element 'g' represents the coupling strength between two electronic eigen states via a phonon. The larger its magnitude, the greater is the probability of the corresponding event happening. But the expression does not take into account the energies of the corresponding eigen states; hence delta functions are used to ensure that only the events which satisfy the energy conservation are included in the summation in Eq. (2). These delta functions are approximated by a Lorentzian of finite width (η) during the summation. To obtain convergence with respect to this width η, the summation must be carried over dense grids of the order 1000×1000×1. Direct calculation over such dense grids poses challenges in terms of computational time and storage capacity. Hence we employ Fourier interpolation based on Wannier functions, which interpolate the values of energies and coupling elements computed using a coarse grid. This part of the calculations is performed through the EPW package[24]. The first half of the expression within the square brackets in Eq. (2) indicates phonon absorption whereas the second half includes phonon emission processes. Since we are interested in the electron scattering rates in the linear regime near the Dirac point, the summation over the phonon wave vectors q is restricted only to the vicinities of the Γ and K points.

The electron scattering rates calculated at 300 K as a function of energy in the K-Γ direction due to different groups of phonons is shown in Fig. 3. Figure 3(a) shows the electron scattering rates due to scattering with the two high energy optical phonons at Γ and K. The inset of Fig. 3 (a) shows a small circular region around Γ over which the summation for the Γ-phonons in Eq. (2) is carried out. The radius of this circle is calculated by considering both the energy and momentum conservation principles. The

linear electronic band structure is characterized by $\varepsilon_k = \hbar v_F|k|$ where $\hbar$ is the Planck's constant and v_F is the constant Fermi velocity (=10^6 m/s). For instance, consider an electron undergoing intra-band scattering within the conduction band from an initial energy state of ε_{ik} = 0.6 eV to ε_{jk+q} = 0.4 eV via Γ-LO phonon emission ($\hbar\omega_q$ = 0.2 eV). The maximum phonon wave vector in this case is given by (ε_{ik} + ε_{jk+q})/$\hbar v_F$ which is equal to 0.06 × 2π /a where a is the lattice constant. The inset also shows the inter-band and intra-band scattering of electrons within the K-point valley due to phonons at Γ. The scattering rates plotted in Fig. 3 include both intra-band (within the conduction band) and inter-band (from conduction band to valence band) interactions. As mentioned before, the scattering due to the out-of-plane (ZA, ZO) phonon modes is negligible. Fig. 3 (b) shows the same for the two other phonon groups Γ-LA/TA and K-LA/LO.

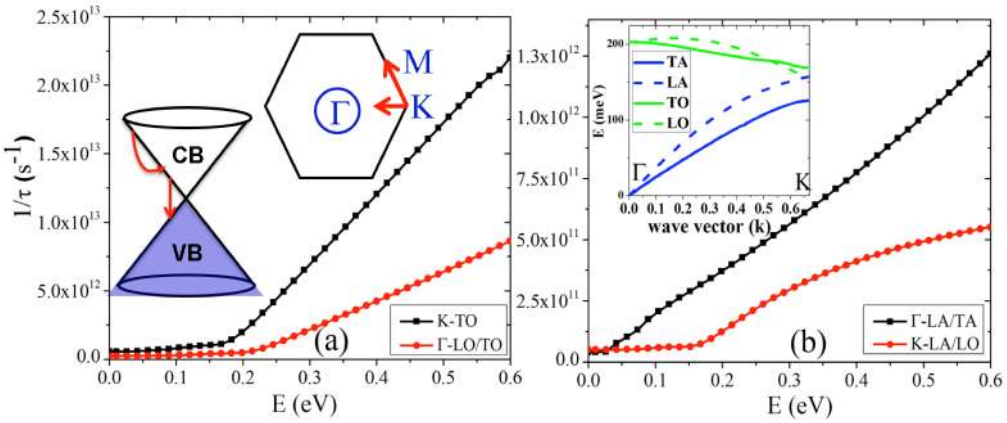

Figure. 3. Electron scattering rate (s^{-1}) as a function of energy in the K-Γ direction due to (a) optical phonon groups Γ-LO/TO and K-TO (b) Γ–LA/TA and K-LA/LO. (Insets in (a) show the intraband and interband interactions in a Dirac cone and the BZ along with points of high symmetry labeled. The inset in (b) shows the in-plane phonon dispersion of graphene.

The scattering rates in the K-M direction are also identical to that of the K-Γ. Hence the scattering rates are considered isotropic for the electronic states around the Dirac point. It can be noticed from the Fig. 3 that the scattering rates vary linearly with energy for both acoustic and optical phonons. This is because as the energy increases, the DOS also increases linearly. As a result, the number of available final states for electrons also increases accordingly with energy as one move away from the Dirac point. The scattering rate due to optical phonons dominate that due to acoustic phonons above the

threshold energy (0.2 eV for Γ-E2g, 0.165 eV for K-A′, and 0.157 eV for K-E′ phonon modes). Below this value, the optical phonon emission process is mostly suppressed at 300 K due to unavailability of empty states in the valence band. It should be noted that acoustic phonons cannot cause inter-band interactions as they fail to satisfy the energy and momentum conservation rules due to their linear dispersion around Γ point. The interband processes is negligible for optical phonons above their threshold energy values. These results are in good agreement with the published results in literature [19, 25].

Based on our results on the scattering rates, we calculated the deformation potential (DP) parameters to compare with the literature based on the equations shown below

$$\frac{1}{\tau_k} = \left(\frac{k_B}{4\mathrm{h}^3 v_F^2 \rho_m \upsilon_s^2} \right) D_{ac}^2 T E_k$$

$$\frac{1}{\tau_k} = \left(\frac{D_0^2}{4\rho_m \omega_o (\mathrm{h}\upsilon_F)^2} \right) \begin{Bmatrix} (E_k - \mathrm{h}\omega_o)(N_q + 1)\Phi(E_k - \mathrm{h}\omega_o) \\ +(E_k + \mathrm{h}\omega_o) N_q \end{Bmatrix} \quad (3)$$

The first equation corresponds to the electron-acoustic phonon interaction which is considered elastic due to the low energy of acoustic phonons near the Γ point. Here k is the electron wave vector, k_B is the Boltzmann constant, $\hbar$ is the reduced Planck's constant, v_F is the Fermi velocity (= 10^6 m/s), ρ_m is the mass density (= 7.6×10^{-7} Kg/m^2) ,υ_s is the average sound velocity of acoustic phonons (= 17 Km/s), D_{ac} is the DP parameter which signifies the coupling strength of electron-acoustic phonon interaction, T is the temperature (= 300 K) and ε_k is the energy of the corresponding electronic eigen state. The second equation corresponds to that of the electron – optical phonon interaction which consists of the phonon emission and absorption, as represented by the first and second terms respectively. Here D_0 is the DP parameter, ω_o is the phonon frequency, N_q is the corresponding Bose-Einstein distribution of phonons and the other symbols hold the same meaning as above. By fitting the above equations to our results on scattering rates in Fig. 3, where the initial and final electronic states are restricted to the conduction band, the following parameters are obtained.

TABLE 1: DP parameters of various phonon modes in graphene

Phonon mode	DP parameter

Γ-LA/TA	10.6 eV
Γ-E_{2g} (LO/TO)	11.0 eV/Å
K- A′ (TO)	16.0 eV/Å
K- E′ (LA/LO)	3.0 eV/Å

Mobility is a property which is very important for devices in nano-electronics. It governs the motion of electrons under an applied electric field. Here, we calculated the intrinsic electron mobility (μ) in graphene at 300 K based on the scattering rates using Boltzmann theory as a function of carrier concentration as demonstrated in Eq. (4) below.

$$\mu = \frac{e v_F^2}{2n}\int_0^E D(\varepsilon)\left(\frac{-\partial f}{\partial \varepsilon}\right)\tau(\varepsilon)d\varepsilon$$

$$n = \int_0^E D(\varepsilon) f(\varepsilon) d\varepsilon \,; D(\varepsilon) = \frac{2\,|\,\varepsilon\,|}{\pi(\mathrm{h}v_F)^2} \qquad (4)$$

In Eq. (4), e is the electrical charge, v_F (=1×10^6 m/s) is the Fermi velocity, n is the carrier concentration, $D(\varepsilon)$ is the electron density of states as a function of electron energy ε, f is the Fermi-Dirac distribution of electrons, and τ is the electron relaxation time. The expressions for carrier concentration and electron DOS are also shown in Eq. (4). The electron mobility in graphene as a function of carrier concentration at 300 K is plotted in Fig. 4. We vary the carrier concentration by shifting the Fermi level (E_f) up into the conduction band. It can be noticed from the figure that the mobility varies inversely with increasing carrier concentration. This is because of the decrease in the average relaxation time, which is proportional to the product inside the integral in Eq. (4). Although optical phonon emission does not contribute to scattering close to the Fermi level, we observe that the contribution of optical phonon absorption is not negligible in addition to the contribution of acoustic phonons. Inter-band processes become irrelevant as E_f shifts into the conduction band. The integral is carried out in the linear regime from 0 to 1 eV although the parameter $\partial f/\partial\varepsilon$ is non-zero only near the Fermi level.

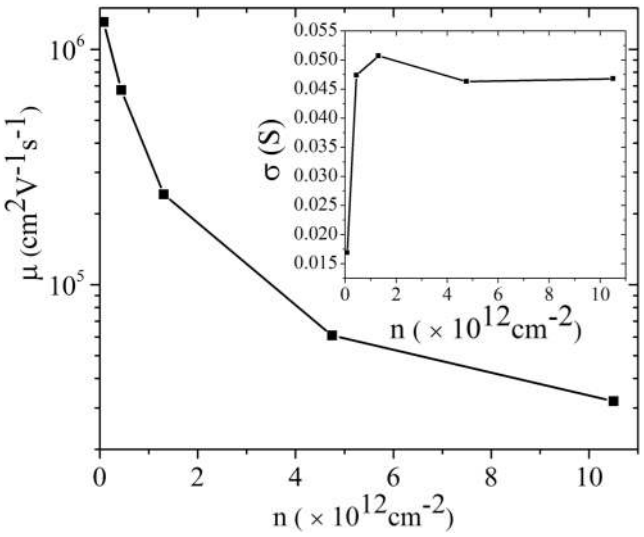

Figure. 4: Mobility (μ) of graphene as a function of carrier concentration (n) at 300 K.

We also calculate the electrical conductivity (σ) from mobility as $\sigma = ne\mu$, which is plotted in the inset of Fig. 4. For intrinsic graphene (E_f at Dirac point = 0 eV), the room temperature value of σ is 0.0169 Siemens, which is approximately about $400e^2/h$. This value is almost two orders of magnitude higher than the experimental measurements on suspended graphene, mainly due to the presence of dominant charged impurity and other short and long-range disorders in these experiments that are not included in our calculations. As inter-band scattering processes becomes irrelevant with increase in E_f (and thereby n), σ increases and eventually becomes constant. These values of μ and σ are due to intrinsic phonon scattering only and establish the upper limit on the values that can be obtained in experiments. The electronic thermal conductivity (κ_e) in graphene is calculated from the classical theory by integrating over the energy space in the linear regime as shown below.

$$\kappa_e = \frac{1}{2}\int_0^E C_e v_e^2 \tau(\varepsilon) d\varepsilon = \frac{v_F^2}{2}\int_0^E \frac{df}{dT_e} D(\varepsilon)\,\varepsilon\,\tau(\varepsilon) d\varepsilon \qquad (5)$$

where C_e is the electronic specific heat defined as the derivative of the electronic energy with respect to the electron temperature (T_e), v_e is the electronic velocity which is equal to the Fermi velocity (v_F) of electrons, τ is the relaxation time, f is the F-D distribution, D is the density of states defined earlier. The value of κ_e calculated with the expression in Eq. (5) using the scattering rates shown above yields a value

of 360 W/mK. After calculating κ_e, we calculated the Lorentz number (L) defined as $\kappa_e/\sigma T$ which comes out to be 2.39×10^{-8} $(V/K)^2$ which is close to the standard value used for metals (2.44×10^{-8} $(V/K)^2$. This validates the applicability of the Wiedemann-Franz (W-F) law to graphene near room temperature. A recent experimental study has measured κ_e to be 10 W/mK at room temperature which is much lower than the value we obtain. We believe this is mainly because of impurities present in the experimental samples. Also, applying the W-F law to the experimentally obtained values of electrical conductivity yields an electronic thermal conductivity (κ_e) of about 5.4 W/mK which is in better agreement with experiments.

After calculating the coupling matrix elements, we predict the rate of electron energy loss due to the four different phonon groups (Γ-LO/ TO, Γ-LA/TA, K-TO and K-LO/LA) in intrinsic graphene as a function of their temperatures. This quantity is computed using the following expression [20, 26]:

$$E_{e-ph} = 4\left(\frac{2\pi}{\hbar}\right)\sum_{k,q,v} \hbar\omega_q^v \left|g_{k,q}^v\right|^2 S(k,q)\delta\left(\varepsilon_{k+q} - \varepsilon_k - \hbar\omega_q^v\right) \quad (6)$$

Here $\hbar$ is the Planck's constant, ω_q is the frequency of phonon at wave vector q and polarization v, $g_{k,q}$ is the e-ph coupling matrix element defined in Eq. (1), ε_k and ε_{k+q} are the electron energies at wave vectors k and $k+q$, $S(k,q)$ is known as the thermal factor defined as

$$S(k,q) = f_{k+q}(1-f_k)(N_q+1) - f_k(1-f_{k+q})N_q$$

where f and N denote the Fermi-Dirac and Bose-Einstein distributions evaluated at the corresponding wave vectors k, q and $k+q$. The indices i,j are dropped above for convenience but the summation over them exists in Eq. (6). This factor represents the net change in the corresponding phonon occupation number (N_q). Under the energy conservation condition imposed by the delta function in Eq. (6), the thermal factor simplifies to a product of the term $[N_q(T_e)\text{-}N_q(T_{ph})]$. This term can be simplified further and can be written simply as the difference between T_e and T_{ph} which facilitates expressing $E_{e\text{-}ph}$ as $G(T_e\text{-}T_{ph})$ where G is defined as the e-ph coupling coefficient [27]. This approximation is widely used for metals which typically have low Debye temperature T_D. But it cannot be used for materials like graphene whose T_D is greater than 1000 K. Hence, in the current study, we calculated the rate of energy exchange term

directly from equation (2) using DFPT as a function of T_e and T_{ph} without any further simplifications, and the results are shown in Fig. 5.

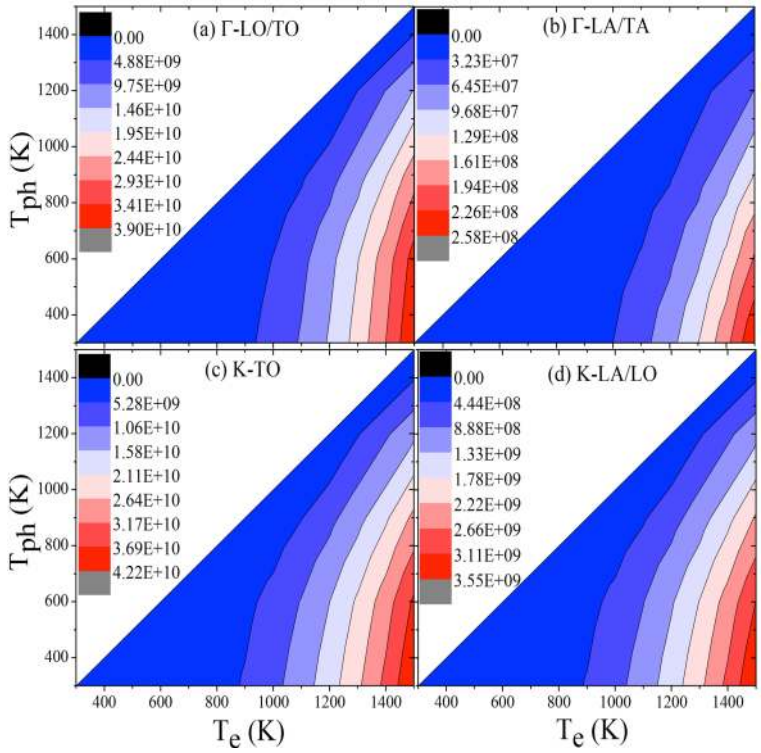

Figure 5. Rate of energy loss (W/m^2) between electrons and the four phonon groups as a function of T_e (horizontal axis) and T_{ph} (vertical axis).

It can be noticed that as the temperature difference between T_e and T_{ph} increases, the magnitude of $E_{e\text{-}ph}$ also increases in a non-linear fashion and drops to zero as T_e approaches T_{ph}. A width (η) of 0.01 mRy is used in these calculations to satisfy the energy conservation conditions. Here, we consider a dense mesh of 8000×8000×1 over the entire BZ for the electron wave vector (k) grid, the sum over which is restricted only to the vicinity of the Dirac points. Summation over such dense meshes is performed by Wannier interpolation using the EPW package [28]. All the relevant terms like the energies and matrix elements are calculated directly from DFPT. The magnitude of $E_{e\text{-}ph}$ of the degenerate Γ-E_{2g} (LO/TO) is comparable with that of the K-A´ (TO) mode. It should be noted that the contribution of the K-E' mode, which denotes the two degenerate modes LA and LO at the K-point, is not negligible. It is weakly coupled to electrons compared to the TO mode at K, but stronger than the acoustic phonons at Γ. The

optical phonon interaction clearly dominates over the acoustic phonons above 300 K by almost 2 orders of magnitude. To the best of our knowledge, this is the first time that these values have been calculated directly from DFT without the deformation potential approximation.

Finally, we aim to obtain the spatial temperature profiles of all energy carriers under laser irradiation using a diffusive model, which is an extension of the standard two temperature model (TTM) [29]. Considering that the laser spot size is on the order of 1μm and the graphene size is several microns, the assumption of diffusive transport for the carriers is reasonable. Instead of assuming a single temperature for all phonon modes, which was commonly done in deriving thermal conductivity from Raman measurements, we assign a separate temperature to each of the phonon polarizations. As it is impossible to obtain the temperature distribution of each carrier in experiments precisely, our model may offer new insights into the carrier non-equilibrium. The governing equations of our diffusive multi-temperature model (DMTM) are shown below in Eq. (7).

$$\begin{aligned}
&\nabla.(\kappa_e \nabla T_e(x,y)) - \sum_{\substack{i=LA,LO,\\ TA,TO}} E_{e-i}(x,y) = S_{laser}(x,y) \\
&\nabla.(\kappa_i \nabla T_i(x,y)) + \sum_{\substack{i=LA,LO,\\ TA,TO}} E_{e-i}(x,y) - \sum_{\substack{i=LA,LO,\\ TA,TO}} E_{i-LAT}(x,y) = 0 \\
&\nabla.(\kappa_j \nabla T_j(x,y)) + \sum_{j=ZA,ZO} E_{j-LAT}(x,y) = 0
\end{aligned} \tag{7}$$

The first term in these equations represents diffusion of energy in the physical domain whereas the remaining terms represent the coupling between the various carriers and is responsible for energy transfer among them. Here $\kappa_{e(i)}$ is the electron (phonon) thermal conductivity, $T_{e(i)}$ is the electron (phonon) temperature as a function of the 2D spatial coordinates x and y. The second term E_{e-i} represents the coupling of electrons to each of the four in-plane phonon modes whose temperatures are governed by the second equation, and their magnitudes can be found in Fig. 5. The external laser source term is denoted by S_{laser} on the right hand side and has Gaussian form $Aexp\{-b(x^2+y^2)\}$. The constants A and b represent the magnitude and the spatial extent (laser spot size) of the source.

Here, we associate one temperature with each of the six phonon polarizations. The second equation in (7) governs the temperature of the in-plane phonon modes. The second term represents the energy gain from electrons and the last term $E_{i\text{-}j}$ represents the coupling of each of the in-plane phonons to other phonon polarizations including the out-of-plane phonons (ZA, ZO). The energy exchange between the six different phonon modes occur via a thermal reservoir represented by the lattice temperature (T_{LAT}) due to the ph-ph scattering processes. The magnitude of this term is computed using the relaxation time approximation (RTA) as

$$E_{i-LAT} = \frac{C_i(T_i - T_{LAT})}{\tau_i} \tag{8}$$

where C_i and τ_i represents the specific heat and relaxation time of mode i as a function of its temperature (T_i) respectively. The calculation of the thermal conductivities of each polarization (κ_i) and the corresponding relaxation times are explained briefly in the supplemental information and with more details in our earlier work [30, 31].

The RTA term in Eq. (8) merely facilitates the redistribution of energy among different phonon modes, so there is no net energy change due to this term. The lattice temperature (T_{LAT}) is computed by equating the sum of six phonon scattering terms to zero. The third equation in (7) represents the transport and scattering of out-of-plane phonons (ZA, ZO). These modes do not couple with electrons but receive energy from other phonon modes. These equations have the same form as that for in-plane phonons. The readers should notice that all the significant processes responsible for energy propagation within the intrinsic graphene layer, including diffusion, e-ph scattering and ph-ph scattering, are included in our model. It should be noted that, in addition to dependence on phonon branches, e-ph and ph-ph scattering processes are also wave vector dependent. In this work we have not treated this dependence explicitly, but only in an average sense on a branch-wise basis. After obtaining all the relevant quantities, the set of equations in (7) are solved by discretizing them over a 2D square mesh of size 5 × 5 μm using the finite volume method (FVM). The calculated e-ph and ph-ph scattering terms and phonon thermal conductivities serve as inputs to our DMTM. Although we estimate the intrinsic value of κ_e to be 360

W/mK, we used a κ_e value of 5.4 W/mK reported in a recent experimental study on high quality suspended graphene[32], in order to compare our results with experiments. We note that the presence of electron-charged impurity scattering does not affect the phonon generation rates. Isothermal boundary conditions are used on the left and right sides representing the heat sink at ambient temperature whereas adiabatic boundary conditions are used on the top and bottom. This is a replica of the single layer graphene suspended across a trench as done in experiments[6]. We also observed that the boundary condition would have no significant bearing on our final conclusions. The coupled equations for electrons and phonons are solved for a laser source of 0.1 mW and a laser spot radius of 0.5 μm which are comparable to experiments iteratively until convergence is achieved using a Gauss-Seidel solver. The resulting temperature and the corresponding heat transfer rate profiles of all the energy carriers are plotted in Fig. 6.

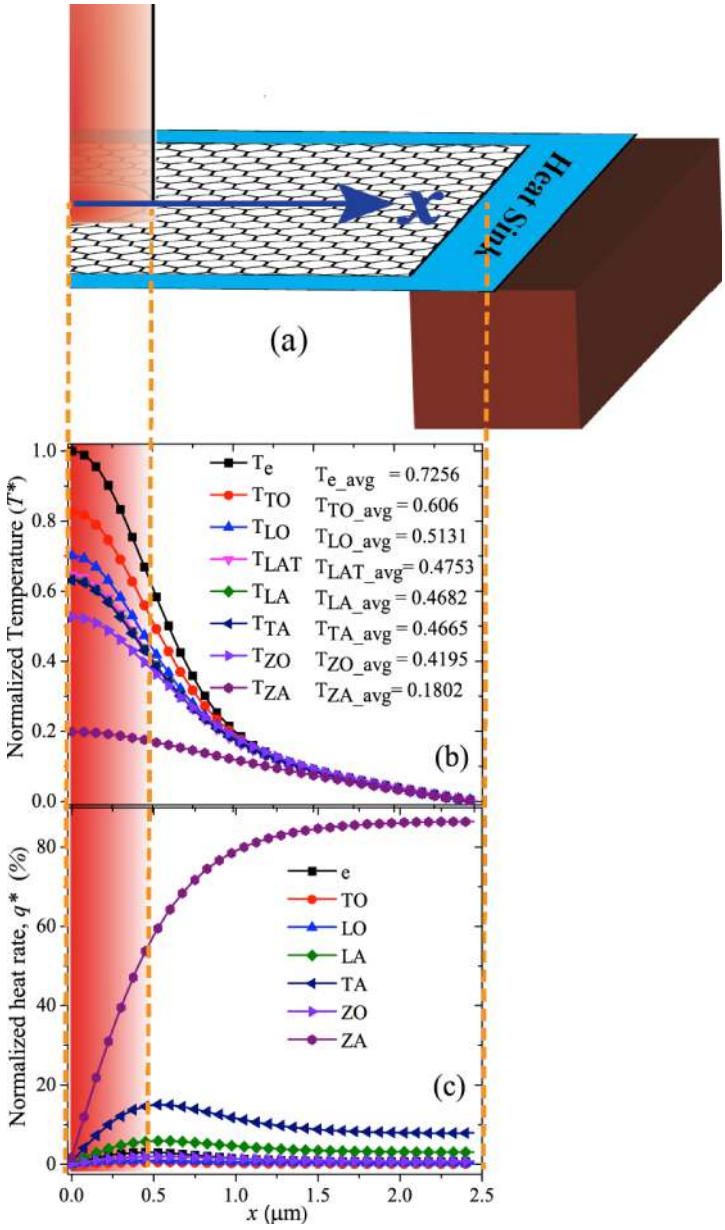

Figure 6. (a) Schematic of half of the Raman spectroscopy experimental domain for characterizing suspended graphene thermal conductivity. Variation of (b) normalized temperature ($T^*=\{T-T_o\}/\{T_{max}-T_o\}$) and (c) Normalized heat current ($q^* = q/q_{in}$) of all the energy carriers from the center of hot spot to the boundary.

Since the laser source is symmetric with intensity decreasing exponentially from the center, the temperature profile also exhibits a similar behavior. The panel Fig. 6(b) shows the spatial variation of the normalized temperature from the spot center to the boundary for all the carriers (electrons and 6 different polarizations of phonons) and the lattice temperature; the latter is the effective average temperature of all

the phonon modes. The normalized temperature T^* is defined as $(T-T_o)/(T_{max}-T_o)$ where T_{max} is the maximum temperature of all the carriers at the center and T_o is the ambient temperature at the heat sink. The actual temperature distribution contour is shown in the supplementary information[36].

The average temperatures of each of the carriers within the laser spot are given in the inset of each of the panels. This figure is the most important finding of our work. The temperature of the TO phonons is closest to that of the electrons, followed by LO phonons. It is not surprising to observe that optical phonons are at higher temperature than acoustic phonons due to their stronger coupling with electrons. The energy from electrons which is dumped into the in-plane phonons ($E_{e\text{-}ph}$) is then redistributed among the other phonon groups as they propagate towards the boundary through ph-ph scattering. The out-of-plane (ZA, ZO) phonon groups receive energy from the in-plane phonon groups and not directly from electrons. The ZA phonons are found to be in strong non-equilibrium with other phonon groups due to their weak coupling with other carriers. We also considered a wider range of laser spot power (0.01-1 mW), and the predicted temperature profiles shown in the supplementary information also reveal a similar degree of non-equilibrium, indicating that carrier non-equilibrium is a general outcome for graphene irradiated with a laser regardless of laser intensity[36].

Since ZA phonons have a high κ compared to other phonon groups (Fig. B1 in supplemental information), they transfer more energy by diffusion than the other phonon groups. This trend can be clearly observed in Fig. 6 (c) where normalized heat rate ($q^*=q/q_{in}$, q_{in} is the total laser power absorbed by graphene) profiles of electrons and various phonon branches are plotted. It indicates the steady increase in the amount of energy carried by the ZA phonons as we move from the center towards the heat sink boundary due to the transfer of energy from other phonons. The contribution of each carrier in terms of percentage of heat carried to the boundary is obtained from this plot and is highlighted in Fig.1 (b) in bold black characters. Now we can estimate the error in Raman measurement of thermal conductivity. If the ratio of intensities is used, the average optical phonon temperature over the hot spot is measured, which is then used in the calculation of κ by solving the equation $\kappa\nabla^2 T + S_{laser} = 0$. In our simulations,

we know the absorbed laser power and the average optical phonon temperature in the laser spot from Fig. 6 (b), so using a similar approach would yield a lattice thermal conductivity of approximately 1200 W/mK. It is significantly lower than the actual value of 3130 W/mK which is the sum of all the individual phonon conductivities used as input parameter in Eq. (3) (based on our earlier calculations). The main reason why the predicted thermal conductivity is lower than the actual by a factor of 2.6 is that the temperature rise of optical phonons is significantly higher than the actual temperature rise of the acoustic (especially ZA) phonons. This clearly shows that the non-equilibrium among the energy carriers in graphene leads to under-estimation of κ in experiments. On the other hand, if the Raman peak shift is used, the measured temperature is that of the intermediate frequency phonons[13] and the analysis of error is more complicated. It is reasonable to assume that the temperature of the intermediate frequency phonons is similar to the lattice temperature in Fig. 6(b), and using it instead of the optical phonon temperature in the above calculation still results in the under-prediction of k by more than twice.

We note that the degree of non-equilibrium obtained above corresponds to a typical case, and in fact it can vary to some extent depending on experimental conditions as well as some assumptions. One factor is the laser intensity and spot size. While we have shown above that the degree of non-equilibrium is not much impacted by different laser intensities, we expect that it will decrease as the spot size increases, since the optical phonons will have more space to interact with acoustic phonons. A second factor is the relative contributions of different phonon modes to the thermal conductivity. Some recent studies have reported that all the three acoustic phonons (LA,TA,ZA) contribute almost equally to the total κ [33, 34], which is different from the case we used here that ZA contributes up to 85 %. We have checked that if the three acoustic modes were to contribute equally, the degree of non-equilibrium is as shown in the supplemental Fig. C3[36]. Following the earlier procedure based on this temperature profile, we estimate that κ is still under-predicted by Raman measurements by a factor of about 1.8 if the intensity ratio is used, and a factor of 1.35 if the peak shift is used. Other factors like he presence of defects and impurities should alter the non-equilibrium to some extent too. We believe this carrier non-equilibrium would in general affect the measured values of κ. This is especially important for 2D materials which

have a weaker coupling between in-plane and out-of-plane phonon modes than 3D materials. It is desirable for experimentalists to account for this non-equilibrium among phonon modes in their derivation of the thermal conductivity, or alternatively, modify the experimental design to minimize the non-equilibrium to a negligible level. . On the other hand, the micro-device approach uses electro-resistive heating and hence does not suffer from the issue of strong electron-optical phonon-acoustic phonon non-equilibrium [35]. However, the measurement is much more difficult than the Raman approach.

4. Conclusion

To conclude, we have assessed the validity of Raman measurements of the thermal conductivity of single layer graphene by calculating electron-phonon and phonon-phonon scattering rates. Electron cooling rates due to scattering on individual phonon groups are calculated directly from DFT. Along with the results obtained on ph-ph scattering rates, we resolved the spatial temperature distribution of all the carriers within the graphene sheet under steady state laser irradiation using a diffusive model. ZA phonons appear to be in strong non-equilibrium with electrons and the other phonon modes. This non-equilibrium is not accounted for in experiments, and as a result, leads to underestimating κ by a factor of 1.35 to 2.6 at room temperature, depending on experimental conditions and assumptions used. Future experimental measurements of the non-equilibrium temperatures of different modes of phonons are highly desirable, to understand the carrier non-equilibrium completely and thereby to accurately estimate thermal conductivity. Also, in this work we did not include any wave vector dependence for the phonons in this model, although including it would cause additional non-equilibrium since the e-ph scattering is restricted only to the vicinity of Γ and K points for the in-plane phonon modes. A more rigorous approach like Boltzmann transport equation (BTE) is essential to include the effects of wave vector and ballistic transport.

Author Information:

Corresponding Author: Xiulin Ruan*, Email: *ruan@purude.edu.

Present Address: 585 Purdue Mall, Department of Mechanical Engineering, Purdue University West Lafayette, IN 47905.

Author Contributions: X.R., J.Y., generated the idea behind this research; A.K.V., performed significant part of the research; H.B and D.S. contributed with their previous experience and offered inputs. A.K.V. wrote the manuscript with inputs from X.R and J.Y.

ACKNOWLEDGEMENTS

The authors would like to acknowledge the insightful discussions with Dr. Li Shi at University of Texas at Austin and Dr. Bo Qiu at Intel Corporation. AKV and JYM acknowledges the financial support by the Robert V. Adams Endowment at Purdue University. XR acknowledges partial support from the Air Force Office of Scientific Research (Grant No. FA9550-11-1-0057). HB acknowledges the support of the National Natural Science Foundation of China (No. 51306111) and Shanghai Municipal Natural Science Foundation (No. 13ZR1456000).

REFERENCES

[1] N. B. Colthup, L. H. Daly, and S. E. Wiberley, *Introduction to infrared and Raman spectroscopy* (Elsevier, 1990).
[2] D. Graf, F. Molitor, K. Ensslin, C. Stampfer, A. Jungen, C. Hierold, and L. Wirtz, Nano letters **7**, 238 (2007).
[3] H. Ramakrishna Matte, A. Gomathi, A. K. Manna, D. J. Late, R. Datta, S. K. Pati, and C. Rao, Angewandte Chemie **122**, 4153 (2010).
[4] A. C. Ferrari, Solid State Communications **143**, 47 (2007).
[5] C. Faugeras, B. Faugeras, M. Orlita, M. Potemski, R. R. Nair, and A. Geim, ACS nano **4**, 1889 (2010).
[6] A. A. Balandin, S. Ghosh, W. Bao, I. Calizo, D. Teweldebrhan, F. Miao, and C. N. Lau, Nano Letters **8**, 902 (2008).
[7] J. H. Seol, et al., Science **328**, 213 (2010).
[8] L. Malard, M. Pimenta, G. Dresselhaus, and M. Dresselhaus, Physics Reports **473**, 51 (2009).
[9] S. Ghosh, I. Calizo, D. Teweldebrhan, E. Pokatilov, D. Nika, A. Balandin, W. Bao, F. Miao, and C. Lau, Applied Physics Letters **92**, 151911 (2008).
[10] D. Sun, Z.-K. Wu, C. Divin, X. Li, C. Berger, W. A. de Heer, P. N. First, and T. B. Norris, Physical Review Letters **101**, 157402 (2008).
[11] W. Cai, A. L. Moore, Y. Zhu, X. Li, S. Chen, L. Shi, and R. S. Ruoff, Nano Letters **10**, 1645 (2010).
[12] J.-U. Lee, D. Yoon, H. Kim, S. W. Lee, and H. Cheong, Physical Review B **83**, 081419 (2011).
[13] N. Bonini, M. Lazzeri, N. Marzari, and F. Mauri, Physical Review Letters **99**, 176802 (2007).
[14] D. Singh, Purdue University (2012).
[15] S. Berciaud, M. Y. Han, K. F. Mak, L. E. Brus, P. Kim, and T. F. Heinz, Physical Review Letters **104**, 227401 (2010).
[16] D.-H. Chae, B. Krauss, K. von Klitzing, and J. H. Smet, Nano Letters **10**, 466 (2009).
[17] Y. Wang, X. Ruan, and A. K. Roy, Physical Review B **85**, 205311 (2012).
[18] C.-H. Park, F. Giustino, C. D. Spataru, M. L. Cohen, and S. G. Louie, Physical Review Letters **102**, 076803 (2009).
[19] K. Kaasbjerg, K. S. Thygesen, and K. W. Jacobsen, Physical Review B **85**, 165440 (2012).

[20] T. Low, V. Perebeinos, R. Kim, M. Freitag, and P. Avouris, Physical Review B **86**, 045413 (2012).
[21] H. J. Monkhorst and J. D. Pack, Physical Review B **13**, 5188 (1976).
[22] P. Giannozzi, et al., Journal of Physics: Condensed Matter **21**, 395502 (2009).
[23] S. Piscanec, M. Lazzeri, F. Mauri, A. Ferrari, and J. Robertson, Physical Review Letters **93**, 185503 (2004).
[24] J. L. Manes, Physical Review B **76**, 045430 (2007).
[25] K. Borysenko, J. Mullen, E. Barry, S. Paul, Y. Semenov, J. Zavada, M. B. Nardelli, and K. Kim, Physical Review B **81**, 121412 (2010).
[26] P. B. Allen, Physical review letters **59**, 1460 (1987).
[27] Z. Lin, L. V. Zhigilei, and V. Celli, Physical Review B **77**, 075133 (2008).
[28] J. Noffsinger, F. Giustino, B. D. Malone, C.-H. Park, S. G. Louie, and M. L. Cohen, Computer Physics Communications **181**, 2140 (2010).
[29] S. I. Anisimov and B. Rethfeld, in *Nonresonant Laser-Matter Interaction* (International Society for Optics and Photonics, 1997), p. 192.
[30] D. Singh, J. Y. Murthy, and T. S. Fisher, Journal of Applied Physics **110**, 094312 (2011).
[31] D. Singh, J. Y. Murthy, and T. S. Fisher, Journal of Applied Physics **110**, 044317 (2011).
[32] S. Yiğen, V. Tayari, J. Island, J. Porter, and A. Champagne, Physical Review B **87**, 241411 (2013).
[33] L. Chen and S. Kumar, Journal of Applied Physics **112**, 043502 (2012).
[34] A. Alofi and G. Srivastava, Journal of Applied Physics **112**, 013517 (2012).
[35] L. Shi, D. Li, C. Yu, W. Jang, D. Kim, Z. Yao, P. Kim, and A. Majumdar, Journal of Heat Transfer **125**, 881 (2003).
[36] Supplemental Information